Origin of the open circuit voltage of plastic solar cells

Brabec, C.J.; Cravino, A.; Meissner, D.; Sariciftci, N.S.; Fromherz, T.; Rispens, M.T; S&#65533;nchez, L.; Hummelen, J.C.; Sanchez, L.

Published in:
Advanced Functional Materials

DOI:
10.1002/1616-3028(200110)11:5<374::AID-ADFM374>3.0.CO;2-W

ADVANCED FUNCTIONAL MATERIALS

FULL PAPER

Origin of the Open Circuit Voltage of Plastic Solar Cells

By *Christoph J. Brabec*,* *Antonio Cravino*, *Dieter Meissner*, *N. Serdar Sariciftci*, *Thomas Fromherz*, *Minze T. Rispens*, *Luis Sanchez*, and *Jan C. Hummelen*

A series of highly soluble fullerene derivatives with varying acceptor strengths (i.e., first reduction potentials) was synthesized and used as electron acceptors in plastic solar cells. These fullerene derivatives, methanofullerene [6,6]-phenyl C_{61}-butyric acid methyl ester (PCBM), a new azafulleroid, and a ketolactam quasifullerene, show a variation of almost 200 mV in their first reduction potential. The open circuit voltage of the corresponding devices was found to correlate directly with the acceptor strength of the fullerenes, whereas it was rather insensitive to variations of the work function of the negative electrode. These observations are discussed within the concept of Fermi level pinning between fullerenes and metals via surface charges.

1. Introduction

Photovoltaic elements based on thin polymer films of solid state composites of conjugated polymer/fullerene compounds seem to be promising candidates for solar energy conversion.[1–3] The mechanical flexibility of plastic materials is welcome for all photovoltaic applications on curved surfaces. By casting thin, semitransparent polymer photovoltaic films between the glass panes of insulated windows, large, unused areas can be accessed, in addition to the limited roof areas of crowded cities. Even the bandgap of the polymer, i.e., the color of such photovoltaic elements, can be varied due to the flexibility of organic synthesis, and the chemical tailoring of desired properties.

An important step towards efficient organic solar cells was the development of the bulk-heterojunction concept.[1] In contrast to bilayer devices, which are comprised of donor and acceptor layers spatially separated, in analogy to the classical p–n junction, the bulk-heterojunction overcomes the limitation of the charge generation at a two-dimensional interface by distributing the acceptor more or less homogeneously into the donor matrix, thereby generating a three-dimensional network of photoinduced charge generating interfaces. Recently, we have demonstrated that the power conversion efficiency of bulk-heterojunction plastic solar cells (PSCs) produced from a conjugated polymer, poly(2-methoxy-5-(3′,7′-dimethyloctyloxy)-1,4-phenylenevinylene) (MDMO-PPV), and a methanofullerene [6,6]-phenyl C_{61}-butyric acid methyl ester (PCBM) can be improved up to 2.5 % under AM1.5 irradiation, by manipulating the solid state morphology (nanostructure) of the components, as well as that of the blend. The results clearly show that the several-fold enhancement in the short circuit current of photovoltaic devices most likely originates from the improved mobility of the charge carriers and from enhanced interfacial contacts between the donor and the acceptor.[4,5]

The excellent photosensitivity and relatively high energy conversion efficiencies obtained from these interpenetrating network bulk-heterojunction materials are promising. One route to enhance the device performance is by understanding the device physics and then optimizing the device parameters. An essential parameter of thin film photovoltaic devices, which influences charge dissociation, charge transport, and charge collection, is the built-in potential. A generally accepted estimate for the built-in potential is given by the open circuit voltage, V_{oc}, which underestimates the built-in potential at room temperature and converges to the correct value at low temperatures. Therefore, the question of the built-in potential is directly related to an extensively discussed phenomenon, the origin of V_{oc}. Mixing fullerenes with conjugated polymers into a composite active layer completely modifies the nature of the thin film devices, compared with those made from conjugated polymers alone,[6,7] and hence the V_{oc} of the corresponding solar cells.[1] Therefore, it is not surprising that models successfully describing the situation in pristine conjugated polymer photodiodes, such as the metal-intrinsic-metal (MIM) or the Schottky junction[9,10] picture, cannot satisfactorily explain the observed V_{oc} in conjugated polymer/fullerene based (*bulk-heterojunction*) solar cells.

In order to investigate the critical parameters influencing the built-in potential in conjugated polymer/fullerene bulk-heterojunction solar cells systematically, a series of highly soluble fullerene derivatives with varying acceptor strengths (i.e., first reduction potentials) was synthesized, and the open circuit voltage of the corresponding devices as a function of acceptor strength was analyzed. These fullerene derivatives, methanofullerene PCBM,[11] a new azafulleroid and a ketolactam quasifullerene (Fig. 1), show a variation of almost 200 mV in their first reduction potentials. Additionally, cells made with [60]fullerene

[*] Dr. C. J. Brabec,[+] A. Cravino, Prof. D. Meissner, Prof. N. S. Sariciftci
Linz Institute for Organic Solar Cells (LIOS), Physical Chemistry
Johannes Kepler University of Linz
Altenbergerstr. 69, A-4040 Linz (Austria)
E-mail: christoph.brabec@e&LS.Siemens.de
Dr. T. Fromherz
Institut für Halbleiter- und Festkörperphysik
Johannes Kepler University of Linz
Altenbergerstr. 69, A-4040 Linz (Austria)
Dr. M. T. Rispens, Dr. L. Sanchez, Dr. J. C. Hummelen
Stratingh Institute and Materials Science Centre, University of Groningen
Nijenborgh 4, NL-9747 AG Groningen (The Netherlands)
[+] Present address: Siemens AG, CT MM1, Innovative Electronics, Paul Gossenstr. 100, D-91052 Erlangen, Germany.

  1616-301X/01/0510-0374 $ 17.50+.50/0

ADVANCED FUNCTIONAL MATERIALS

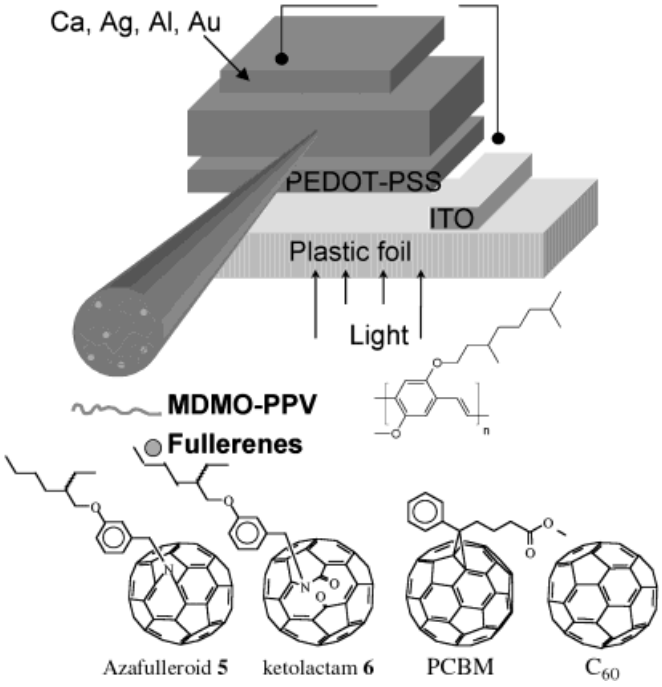

Fig. 1. Chemical structures of the investigated compounds, and device layout of the solar cells.

(C_{60}) were compared. It is important to emphasize that, apart from C_{60}, these acceptors have comparably sized solubilizing groups. Effects due to different donor–acceptor distances, and/or different morphologies, should, in this way, be minimized, as is required for a comparative study. Nevertheless, we realize that it is highly unlikely that the morphologies of the various active layers are identical. (This is unavoidable, however, since it is obviously impossible to alter the electron affinity of an acceptor component without altering its structure!)

MDMO-PPV (Fig. 1) was used as the polymeric donor, in all experiments. This polymer has been used routinely in plastic photovoltaic (PV) research over the last few years.[4,5,12] In the second part of this research, we investigated the possibility of influencing the built-in potential of the photodiodes by varying the work function of the top electrode (i.e., the negative electrode, *collecting* electrons from the active layer). Four different metal electrodes were selected for this purpose: calcium, silver, aluminum, and gold, thus varying the work function by more than 2 eV, while keeping the transparent positive front electrode material constant (i.e., a poly(3,4-ethylenedioxythiophene):poly(styrene sulfonate) (PEDOT:PSS) layer on an indium tin oxide (ITO) coated support material).

2. Results and Discussion

2.1. Synthesis of Two New Fullerene Acceptor Materials

The synthesis of the target molecules [5,6]-*N*-3-(2-ethylhexyloxy)benzyl azafulleroid (**5**) and *N*-3-(2-ethylhexyloxy)benzyl ketolactam (**6**), started with the preparation of 3-(2-ethylhexyloxy)benzyl azide (**4**), as depicted in Scheme 1. Azide **4** was

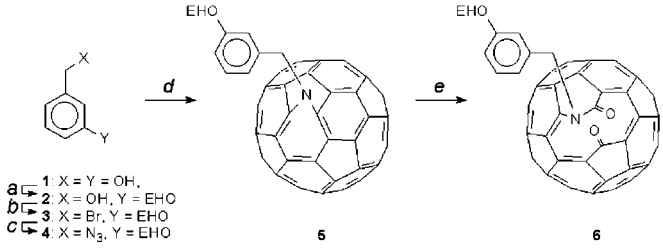

Scheme 1. Synthesis of *N*-3-(2-ethylhexyloxy)benzyl azafulleriod **5** and of *N*-3-(2-ethylhexyloxy)benzyl ketolactam **6**. EHO = 2-ethyl hexyloxy. a) NaOMe, 2-ethyl-1-bromohexane, MeOH, Δ, 16 h, 29 %. b) PBr_3, Et_2O, 3 h, 59 %. c) NaN_3, DMSO, 1.5 h, 95 %. d) C_{60}, ODCB, 180 °C, 2 h, 18 %. e) O_2, halogen lamp, Kapton filter, ODCB, 3 h, room temperature, 18 % (based on [60]fullerene).

synthesized from commercially available 3-hydroxymethylphenol (**1**) by alkylation with 2-ethylhexylbromide,[13] conversion of the benzyl alcohol **2** to a benzyl bromide **3**,[14] followed by reaction with sodium azide in dimethyl sulfoxide (DMSO),[15] all analogously to known procedures. Subsequently, [5,6]-azafulleroid **5** was prepared by the addition of azide **4** to a solution of C_{60} in boiling *o*-dichlorobenzene (ODCB) and subsequent reaction for 2 h at 180 °C, yielding **5** in an optimized yield of 18 %, after column chromatography.

Ketolactam **6** was prepared by self-sensitized photo-oxygenation of azafulleroid **5** (Scheme 1). Since the separation of **5** from C_{60} was difficult, it was more practical to use a partially purified mixture (consisting of **5** and C_{60}) in the photo-oxygenation reaction.[16] The cage-opening reaction, which most likely proceeds via a dioxetane-intermediate, was complete in 3 h, as indicated by high performance liquid chromatography (HPLC). Column chromatography gave **6** in 18 % yield, indicating the conversion of **5** to **6** to be quantitative (see above).

Azafulleroid **5** showed 31 signals for the fullerene-sp^2 carbons in the ^{13}C NMR spectrum, indicative of C_S-symmetry. UV-vis spectroscopy featured the characteristic azafulleroid absorptions [341 nm (ε = 426 000 $M^{-1}cm^{-1}$), 437 nm (sh), 551 nm (ε = 13 900 $M^{-1}cm^{-1}$)] are present.[17] In the Fourier transform infrared (FTIR) spectrum, a strong peak at 525 cm^{-1}, typical for a monosubstituted [60]fullerene, was observed. Matrix-assisted laser desorption ionization time-of-flight mass spectrometry (MALDI-TOF-MS; S_8) gave a M^- at 953.7, in accordance with a calculated value of m/z = 953.2.

Ketolactam **6** showed 57 signals in its ^{13}C NMR spectrum for the fullerene-sp^2 carbons, showing a lack of symmetry compared to **5**. The ketone carbon resonance was found at 194.8 ppm, whereas for the lactam carbon the most likely resonance is either at 160.7 or 159.6 ppm. The ^1H NMR spectrum showed a double doublet for the diasterotopic benzylic hydrogens at δ 6.38 and 5.39 ppm (J = 15 Hz), as a result of the chirality of the cage-opened fullerene. The UV-vis spectrum showed the characteristic absorption pattern for a ketolactam fullerene moiety [333 (ε = 488 000), 433 (44 400), 619 (4 560) and 698 nm (4 410 $M^{-1}cm^{-1}$)], whereas the FTIR spectrum showed absorption features at 1727 and 1689 cm^{-1}, indicative of the ketone and lactam moieties, respectively. Moreover, a peak at 522 cm^{-1}, assigned to the fullerene core, was observed. Both **5** and **6** gave satisfactory elemental analyses.

  1616-301X/01/0510-0375 $ 17.50+.50/0

2.2. Cyclic Voltammetry

The redox behavior of both new fullerene derivatives was determined by cyclic voltammetry (CV), together with that of the parent C_{60} and PCBM, all were measured under identical conditions. The voltammograms are shown in Figure 2, and the data are tabulated in Table 1, for numerical comparison. All four CVs showed four reversible reduction waves corresponding to the reduction of the fullerene cage. However, the first reduction waves—indicative of the electron acceptor strength of the compounds—show distinctive differences. Ketolactam **6** (–0.53 V) appeared to be a substantially better electron acceptor than C_{60} (–0.60 V),[18] whereas azafulleroid **5** (–0.67 V) is close to C_{60}, and PCBM (–0.69 V) showed a clearly diminished electron affinity. In the case of azafulleroid **5**, an additional shoulder to the wave at –2.02 V was observed. We assigned this feature to the reduction of the addend, after comparison to *N*,*N*-dimethyl (3-methoxy)benzyl amine (–1.88 V). The CV of ketolactam **6** showed an additional wave (–1.93 V), which most likely corresponds to the reduction of the ketone moiety. This value compares nicely to that of benzophenone (–1.85 V), observed under the same conditions. Hence, a difference of 160 mV is observed between the strongest and the weakest acceptor. Since, in general, the reduction potential of a compound is solvent dependent, it is the relative *differences* between the acceptor strengths of the fullerene derivatives that are important, and not so much their absolute values. In the discussion below, we will assume that the trend found working with solutions is representative also for the fullerene derivatives in the solid state.

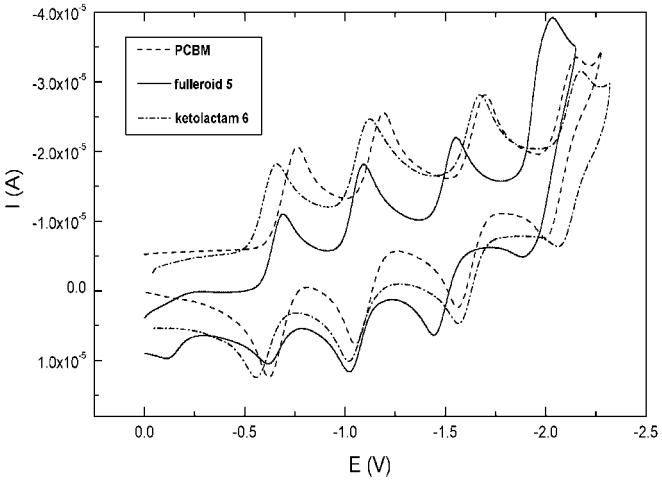

Fig. 2. Cyclic voltammograms of PCBM, azafulleroid **5** and ketolactam **6**. The experimental conditions were the following: reference electrode was a Ag wire; GCE was the working electrode; Bu_4NPF_6 (0.1 M) was the supporting electrolyte; 100 mV/s was the scan rate; ODCB/MeCN (4:1) was the solvent.

Table 1. Redox potentials (*V* vs NHE) of C_{60} and fullerene derivatives [a].

Compound	E^1_{red}	E^2_{red}	E^3_{red}
PCBM	–0.69	–1.09	–1.57
Azafulleroid **5**	–0.67	–1.07	–1.52
Ketolactam **6**	–0.53	–0.93	–1.41
C_{60}	–0.60	–1.01	–1.46

[a] Experimental conditions: Quasi Ag/AgCl wire (calibrated with ferrocene) as reference electrode, Pt foils as working and counter electrodes; Bu_4NPF_6 (0.1 M) as supporting electrolyte; ODCB/MeCN (4:1) as solvent. Scan rate 100 mV/s; room temperature.

The tuning of the reduction potential of fullerene-based materials has also been accomplished by other research groups. Recently, qualitatively comparable results with respect to *increasing* the electron affinity of fullerenes were obtained with isoxazolo-fullerenes,[19] fulleropyrrolidium salts,[20] and certain metal containing fullerene-crown ether conjugates.[21] The possible application of fullerene derivatives in an organic "plastic" solar cell, however, demands processability and a total reversibility of the one-electron reduction. These criteria are met by both azafulleroid **5** and ketolactam **6**. Irradiation of **5** in the presence of oxygen yields **6**. This ketolactam is inert to further photo-oxidation, which in itself is an interesting property for a component in a "plastic" solar cell.

2.3. Photovoltaic Devices

2.3.1. Variation of the Acceptor Materials

Thin film photovoltaic devices with an active layer thickness of ~100 nm were produced by doctor blading the active layer donor–acceptor composite from toluene solutions on top of a PEDOT:PSS (~100 nm)/ITO (80 nm)/polyester (175 μm) substrate. Subsequently, a top aluminum layer was deposited by evaporation. Photovoltaic parameters were determined under inert gas conditions under illumination with 60 mW/cm^2 white light from a halogen lamp. More than 80 devices were produced from each acceptor type to allow a statistical evaluation of the observed open circuit voltage. A box plot diagram was chosen to present the results from current/voltage (*I*/*V*) measurements for the V_{oc} (Fig. 3). The horizontal lines in the box denote the 25th, 50th, and 75th percentile values. The error bars denote the 5th and 95th percentile values. The two symbols below and above the 5th/95th percentile error bars denote

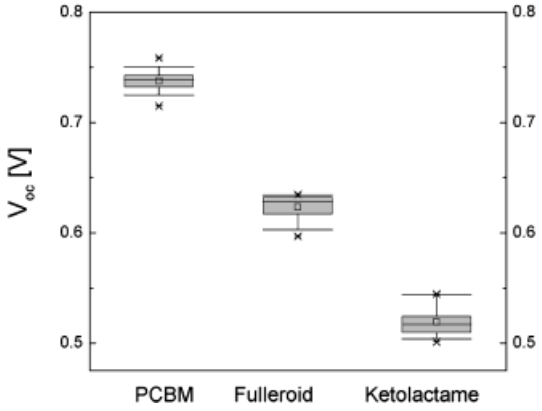

Fig. 3. The V_{oc} for the solar cells utilizing PCBM, azafulleroid **5**, and ketolactam **6** as the acceptor components, in bulk-heterojunction solar cells comprising MDMO-PPV as the electron donor.

  1616-301X/01/0510-0376 $ 17.50+.50/0

the highest and the lowest observed values, respectively. For all three acceptors presented, a relatively narrow distribution of the open circuit voltage was observed, indicating excellent reproducibility: 75 % of the devices from each acceptor are distributed less than 40 mV around their average value. The highest and the lowest average open circuit voltages were observed for the PCBM containing cells and for the ketolactam containing cells, with 760 and 560 mV, respectively.

2.3.2. Variation of Top Electrode Materials

PCBM was chosen as the reference electron acceptor for investigating the influence of the top (negative) electrodes with different work functions on the built-in potential of conjugated polymer/fullerene bulk-heterojunction plastic solar cells. These devices were produced by spin-casting the photoactive donor/acceptor mixture on top of PEDOT:PSS (80 nm)/ITO (100 nm)/glass substrates from toluene solutions. The top electrode materials were evaporated thermally at a vacuum lower than 10^{-6} mbar. Figure 4 shows the *I*/*V* curves of four typical devices utilizing Ca (ϕ_{Me} = 2.87 eV), Al (ϕ_{Me} = 4.28 eV), Ag (ϕ_{Me} = 4.26 eV), and Au (ϕ_{Me} = 5.1 eV)[22] as the negative electrodes: the scale is logarithmic. A total variation of less than 200 mV of the V_{oc} was observed for a variation of the negative electrode work function by more than 2.2 eV. For the devices with a Au electrode, V_{oc} was found to be slightly lower than the average value, but still as high as 650 mV. The Ca devices exhibit a V_{oc} of 814 mV. It is interesting to note that the direction of flow of the short circuit current (i.e., the polarity of the device) was not reversed in the case of the Au electrode, as would normally be expected for a MIM device due to the nominally slightly higher work function of Au compared to the ITO/PEDOT:PSS electrode on the other side. In this device, holes still flow towards the ITO/PEDOT:PSS electrode (positive electrode), while electrons are still collected at the (negative) Au electrode. The observation that the short circuit current I_{sc} for the Au devices is clearly lower than for comparable devices with other electrodes will be discussed later.

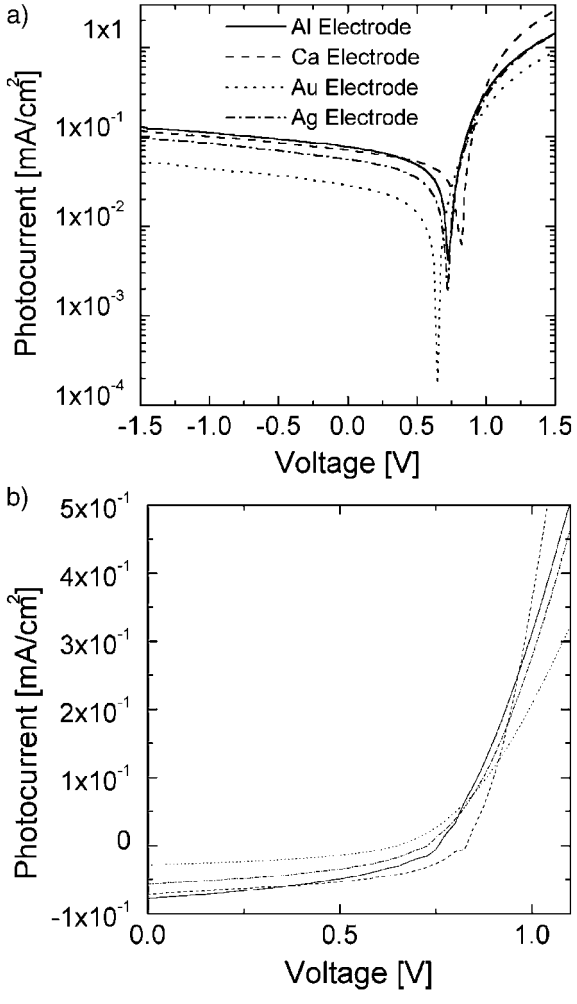

Fig. 4. a) *I*/*V* curves for MDMO-PPV/PCBM photovoltaic devices with different metal electrodes. Al electrode (solid line), Ca electrode (dashed line), Au electrode (dotted line), Ag electrode (dash-dotted line). b) *I*/*V* curves with a linear scale.

2.4. Fermi Level Pinning

The experimental results on the variation of the acceptor strength and on the variation of the top electrode work function are summarized in Figures 5a and 5b. Figure 5a shows the highest observed V_{oc} (from Fig. 3) versus the acceptor strength for devices utilizing PCBM, C_{60}, azafulleroid **5** and ketolactam **6** as electron acceptors. The data points were fitted to a linear model, and a slope of $S_1 \sim 1$ was derived from the fitting proce-

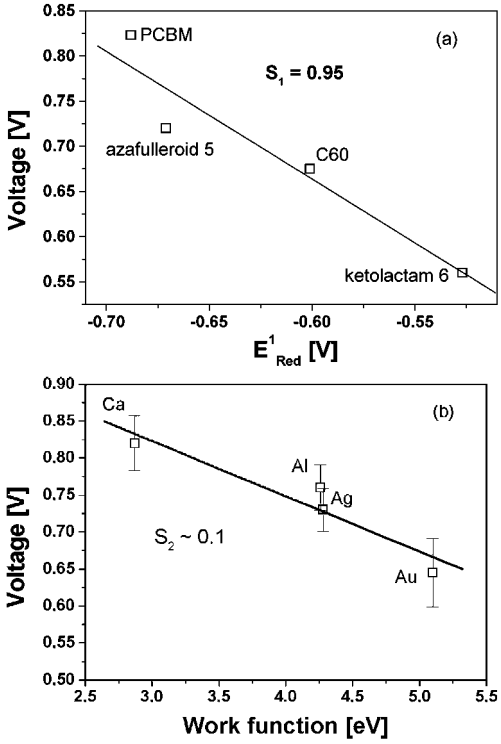

Fig. 5. a) V_{oc} versus acceptor strength and b) V_{oc} versus negative electrode work function. The slopes S_1 and S_2 of the linear fits to the data are given inside the figures.

  1616-301X/01/0510-0377 $ 17.50+.50/0

dure. The fact that a slope of unity was obtained emphasizes the strong coupling of the V_{oc} to the reduction strength of the acceptors, as expected for the ideal case of ohmic contacts between the different fullerenes and the aluminum contact. Deviations from this "ideal behavior" might occur, since the reduction strengths of the acceptors plotted in Figure 5a on the *x*-axis were taken from electrochemical data in solution and not from thin solid films.

The influence of the work function of the negative electrode on the V_{oc} of the MDMO-PPV/PCBM solar cells is shown in Figure 5b. It is important to note that the *x*-axis now covers more than 2 eV. Again, a linear model was fitted to the experimental data and a slope $S_2 \sim 0.1$ was calculated as the best fit. This result shows that the work function of the metal has a considerably weaker effect on the V_{oc} values than does the reduction potential of the fullerene derivative.

In order to understand this behavior, we use a concept that has been developed to explain the built-in potential for inorganic semiconductor/metal interfaces, and which is based on the index of interface behavior *S*.[23] The parameter *S* is defined as the slope of a plot of the blockade potential of a semiconductor/metal interface versus the work function of the metal:

$$qV_B = S(\phi_M - \phi_{SC}) + C \quad (1)$$

where qV_B is the blockade potential of the interface barrier, ϕ_M and ϕ_{SC} are the work functions of the metal and the semiconductor, respectively, and *C* is a constant that describes the interface potential for the ideal ohmic contact. From the results presented above (Figs. 5a and 5b), we propose the following equation for the open circuit voltage in the PSC:

$$V_{OC} = (A_{OX} - S_1 E_{red(A)}) - S_2(\phi_M - E_{red(A)}) + C \quad (2)$$

where, $E_{red(A)}$ is the reduction potential of the acceptor (fullerene derivative) and S_1 and S_2 are the slopes calculated from Figures 5a and 5b. A_{ox} is a constant representing all the contributions from the positive electrode to the V_{oc}, and is expected to be properly described by the oxidation potential of the conjugated polymer. The negative sign in front of the second term of Equation 2 takes into account that this contribution works as a counter diode. Since the parameter S_2 was found to be sufficiently small ($S_2 < 0.1$), it can be also neglected for the open circuit voltage, leading to Equation 3, which yields a good estimation of our results:

$$V_{OC} = (A_{OX} - S_1 E_{red(A)}) + C \quad (3)$$

Comparing Equations 1 and 2, the slope S_2 of the linear fit calculated from Figure 5b resembles the index of interface behavior *S*. Following this concept, the observation of a slope as low as 0.1 in Figure 5b suggests a mechanism called "Fermi level pinning".[23] In such a case, the work function of the metal is pinned to the work function of the semiconductor (typically via surface states), independent of whether the work function of the metal is higher or lower than the Fermi level of the semiconductor. The presence of surface charges leads to band bending at the semiconductor–metal interface. For n-type semiconductors, these states are acceptor-like, and the semiconductor at equilibrium may exhibit an upward (negative) band bending as the surface Fermi level moves toward the charged states. For a p-type semiconductor with donor-like surface states, the semiconductor at equilibrium would exhibit downward band bending as the surface Fermi level moves toward the charged states. For the photodiodes presented in this study, we propose that the Fermi level of the negative electrode metal is pinned to the reduction potential of the fullerene. First, the correlation of the open circuit voltage with the reduction potential of the acceptor (Fig. 5a) proves that the energy alignment of the metal is related to the lowest unoccupied molecular orbital (LUMO) energy states of the acceptor and not of the polymer. Second, recent results from XPS[24,25] (X-ray-photoemission) on mono- and multi-layers of C_{60} on different metals with various work functions showed clearly that there is considerable charge transfer to C_{60} adsorbed on metal surfaces. The alignment of the ground state energies was determined by the interface dipole, i.e., the bond formation in the first layer, which ensures the charged state's induced Fermi level alignment to the substrate. Surface states in organic semiconductors are unlikely due to the weak bonding forces between the molecular units. However, fullerenes, with their cage-like π-electron system and their high tendency to crystallize, may be different, exhibiting strong charge transfer (up to 1.8 electrons per fullerene) at fullerene/metal interfaces.[26] It is beyond the aim of this paper to speculate on the nature of the charged states for thin spin-cast films of fullerenes: this has been discussed for ultra high vacuum (UHV) grown films.[27–29] The presence of large interface dipoles between metals and organic semiconductors has also been shown for a large number of other small molecules.[30]

Assuming that the mechanism of Fermi level pinning is dominant for the contact formation at the negative electrode of the photodiodes, the qualitative difference between the Au electrode and the Ca, Ag, and Al electrodes can be discussed. Whereas the low work function of Ca, Ag, and Al ($\phi_{ME} < 4.3$ eV) will favor ohmic contacts to fullerenes ($E_{Fermi\ (C60)} \sim 4.7$ eV), Au is the only one to form ohmic contacts to a hole-transporting conjugated polymer such as MDMO-PPV, due to its high work function ($\phi_{Au} \sim 5.1$ eV). The other three metals are known to form rectifying (blocking) contacts to the holes in a conjugated polymer.[31,32] For the devices presented in this study, it was shown above that the pinning of the metal work function to the fullerene reduction potential promotes a quasi-ohmic contact between the metal and the fullerene, even for a Au electrode (preceded by charge transfer between the metal and the first fullerene monolayer, yielding an interfacial dipole layer). For the proper function of a photodiode, asymmetric contact conditions are essential. At the negative electrode, an ohmic contact to the electron transporting phase of the donor–acceptor composite is favorable, while the holes should be blocked (rectifying contact). This condition seems to be fulfilled for the photodiodes with a Ca, Ag, or Al negative electrode, due the low value of the work function compared to the Fermi level of the fullerenes. In the case of the negative Au electrode, ohmic contacts may be formed to both the fullerene

  1616-301X/01/0510-0378 $ 17.50+.50/0

ADVANCED FUNCTIONAL MATERIALS

phase and the conjugated polymer phase. Such contacts will enhance surface recombination, thereby reducing the short circuit current and the open circuit voltage. An interesting consequence of the fact that the Au contact to the conjugated polymer phase is a rectifying one for the Au-PSC is the occurrence of a dipole layer at this interface with a reversed sign compared to Al, Ca, and Ag electrodes. This results in positively charged states on the fullerene for the Au contact and in negatively charged states on the fullerene for the other contacts with higher work functions.

3. Conclusion

In conclusion, we have found that the open circuit voltage in plastic solar cells is directly related to the acceptor strength of the fullerenes. This result fully supports the view that the open circuit voltage of this type of donor–acceptor bulk-heterojunction cell is related directly to the energy difference between the HOMO level of the donor and the LUMO level of the acceptor components. Furthermore, and also in full agreement with this view, it was found that a variation of the negative electrode work function influences the open circuit voltage in only a minor way. In accord with results from XPS studies proving surface charges on C_{60} at metal interfaces, this electrode-insensitive voltage behavior is identified as a result of Fermi level pinning between the negative metal electrode and the fullerene reduction potential via charged interfacial states. These observations lead the way to molecular engineering of the open circuit potentials in plastic solar cells by tailoring the electronic structure of the acceptor.

4. Experimental

Device Fabrication: ITO/glass substrates (MDT Darmstadt) and ITO/polyester substrates (Cadillac Plastic, Germany) were cleaned in ultrasonic baths of acetone and isopropanol. Devices for acceptor strength variation were produced by doctor blading. Poly(3,4-ethylenedioxythiophene) doped with polystyrene sulfonic acid (PEDOT:PSS, Bayer AG) was doctor bladed to a thickness of 100 nm on top of the ITO, from a water solution. The active layer was cast from a toluene solution with equal molar ratios of MDMO-PPV and the fullerene (1:1). Deposition of the top electrode was done by thermal evaporation of Al through a shadow mask to define a device area of 5 mm^2. Devices for variation of the negative electrode work function were produced by spin-casting a thin film from a MDMO-PPV/PCBM (1:1 molar ratio) solution from toluene. After drying, the top electrode—Ca, Al, Ag, or Au—was thermally deposited through a shadow mask to define a device area of 7.5 mm^2. All electrodes were non-transparent with a thickness of ~ 80 nm. Spin-casting of the devices was performed under ambient conditions, avoiding exposure to light resonant with the photoactive components, thereby preventing photooxidation [33]. After evaporation of the metal, electrode devices were characterized in a dry-box under an argon atmosphere. *I–V* characteristics were taken with a source-meter (Keithley 2400) while illuminating the devices through the ITO/PEDOT side with 60 mW/cm^2 white light from a halogen lamp.

Synthesis of Azafulleroid and Ketolactam: All reagents and solvents were used as received, or purified using standard procedures. [60]Fullerene (99.5 %) was purchased from Bucky USA and used without purification. All reactions were performed under a nitrogen atmosphere, unless indicated otherwise. Nitrogen was deoxygenated using a copper column. Flash chromatography was performed using Kieselgel Merck Type 9385 (230–400 mesh). Analytical thin layer chromatography (TLC) was performed using aluminum coated Merck Kieselgel 60 F_{254} plates. Melting points were determined with a Mettler FP1 melting point apparatus equipped with a Mettler FP2 microscope. ^1H NMR and ^{13}C NMR spectroscopy were performed on a Varian Unity Plus (500 MHz) instrument, or on a Varian VXR-300 (300 MHz) instrument at 298 K, as indicated. Spectra recorded in CS_2 employed a D_2O insert as the external lock and ^1H reference (δ = 4.67 ppm relative to TMS) for the ^1H NMR, and CS_2 was used as the internal ^{13}C reference (δ = 192.3 ppm relative to TMS) in the ^{13}C NMR. Coupling constants (J) are given in Hz. Multiplicities are denoted as follows: s = singlet, d = doublet, t = triplet, sep = septet, dd = double doublet, m = multiplet, br = broad. FTIR spectra were recorded on a Mattson Galaxy 4020 instrument. UV-vis spectra were recorded on a Hewlett Packard HP 8452 UV-vis spectrophotometer. MALDI-TOF-MS measurements were performed on a Micromass TofSpec E apparatus (negative-ion reflectron mode) by using elemental sulfur as the matrix [34]. Measurements were performed on 1:1 (v/v) aliquots of the analyte (~ 1 mg/mL in CS_2) and the matrix (elemental sulfur: 20 mg/mL). HPLC analyses were performed on a Hewlett Packard HP LC-Chemstation 3D (HP 1100 Series) using an analytical Cosmosil Buckyprep column (4.6 × 250 mm). Cyclic voltammetry was performed using an Autolab PGStat 100 equipped with a BAS C3 cell stand. Elemental analyses were performed by the Microanalytical Department of this laboratory.

3-(2-Ethylhexyloxy)benzyl alcohol (**2**) [13]: Sodium methoxide (4.70 g, 87 mmol) was dissolved in methanol (40 mL), and a solution of 3-hydroxymethyl phenol (9.92 g, 80 mmol) in methanol (50 mL) was added. The clear solution was heated under reflux for 30 min, and subsequently cooled to room temperature. A solution of 2-ethyl-1-bromohexane (17.0 g, 88 mmol) in methanol (50 mL) was added dropwise. The mixture was heated under reflux overnight and subsequently cooled to room temperature. The solvent was removed in vacuo. Final purification was done by column chromatography (silica gel; toluene/methanol = 7:1) giving pure product (5.55 g, 24 mmol, 29 %) as a colorless oil. ^1H NMR ($CDCl_3$, 300 MHz), δ [ppm]: 7.27 (t, J = 8.0, 1H), 6.94–6.91 (m, 2H), 6.85 (dd, J = 8.1, J = 2.1, 1H), 4.66 (br s, 2H), 3.86 d, J = 6.0, 2H), 1.74 (sep, J = 6.1, 1H), 1.55–1.27 (m, 8H), 0.96–0.89 (m, 6H). ^{13}C NMR ($CDCl_3$, 75 MHz), δ [ppm]: 159.62, 142.40, 129.45, 118.76, 113.74, 112.88, 70.40, 65.22, 39.34, 30.49, 29.03, 23.82, 23.00, 14.03, 11.05. FTIR (KBr), ν [cm^{-1}]: approx. 3331 (m, OH), 1264 (s, ArOR), 1037 (m, ArOR), 782 (m, Ar). HRMS: Calcd for $^{12}C_{15}H_{24}O_2$ (M^+): m/z = 236.178. Found m/z = 236.177. Anal. calcd. for $C_{15}H_{24}O_2$: C, 76.23 %; H, 10.23 %. Found: C, 76.32 %; H, 10.28 %.

3-(2-Ethylhexyloxy)benzyl bromide (**3**) [14]: 3-(2-Ethylhexyloxy)benzyl alcohol (5.50 g, 23 mmol) was dissolved in ether (235 mL), and phosphorous tribromide (7.33 g, 27 mmol) dissolved in ether (60 mL) was added. After stirring for 3 h at room temperature, the mixture was poured into water (1.0 L) and extracted with dichloromethane (4 × 500 mL). The combined organic layers were dried over sodium sulfate and evaporated in vacuo. Final purification was done by column chromatography (silica gel; diethyl ether/cyclohexane = 1:1) giving pure **3** (4.10 g; 13.7 mmol, 59 %) as a colorless oil. ^1H NMR ($CDCl_3$, 300 MHz), δ [ppm]: 7.24–7.19 (t, J = 7.8, 1H), 6.95–6.91 (m, 2H), 6.82 (dd, J = 8.3, J = 1.1, 1H), 4.45 (s, 2H), 3.82 (d, J = 6.0, 2H), 1.70 (sep, J = 6.0, 1H), 1.54–1.25 (m, 8H), 0.94–0.87 (m, 6H). ^{13}C NMR ($CDCl_3$, 75 MHz), δ [ppm]: 159.57, 139.00, 129.70, 120.97, 115.05, 114.66, 70.46, 39.37, 33.58, 30.51, 29.07, 23.84, 23.03, 14.06, 11.10. FTIR (KBr), ν [cm^{-1}]: 1266 (s, ArOMe), 693 (m, RBr). HRMS: Calcd for $^{12}C_{15}H_{23}BrO$ (M^+): m/z = 298.093. Found m/z = 298.094. Anal. calcd for $C_{15}H_{23}BrO$: C, 60.21 %; H, 7.75 %; Br, 26.70 %. Found: C, 59.84 %; H, 7.84 %; Br, 26.41 %.

3-(2-Ethylhexyloxy)benzyl azide (**4**) [15]: Sodium azide (990 mg, 15.2 mmol) was dissolved in DMSO (22 mL) by stirring overnight at room temperature. Then 3-(2-ethylhexyloxy)benzyl bromide (4.10 g, 13.7 mmol) was added and the resulting mixture was stirred for 1.5 h. Addition of water (75 mL) and subsequent cooling to room temperature was followed by extraction with ether (3 × 50 mL). The combined organic layers were washed with water (2 × 75 mL) and pre-dried over brine (1 × 75 mL). Drying over sodium sulfate and subsequent evaporation of the solvent in vacuo yielded the azide (3.39 g, 13.0 mmol, 95 %) as a slightly yellow oil, pure enough to allow for the subsequent reaction. ^1H NMR ($CDCl_3$, 300 MHz), δ [ppm]: 7.27–7.21 (m, 1H), 6.88–6.81 (m, 3H), 4.27 (s, 2H), 3.82 (d, J = 5.4, 2H), 1.70 (sep, J = 6.0, 1H), 1.56–1.24 (m, 8H), 0.93–0.86 (m, 6H). ^{13}C NMR ($CDCl_3$, 75 MHz), δ [ppm]: 159.73, 136.74, 129.71, 120.03, 114.32, 114.22, 70.45, 54.73, 39.36, 30.49, 29.05, 23.82, 23.00, 14.03, 11.07. FTIR (KBr), ν [cm^{-1}]: 2099 (s, N_3), 1266 (s, ArOR).

N-3-(2-ethylhexyloxy)benzyl azafulleroid (**5**): C_{60} (1.08 g, 1.5 mmol) was dissolved in ODCB (200 mL), degassed (3 ×), and heated under reflux under a nitrogen atmosphere. 3-(2-Ethylhexyloxy)benzyl azide (408 mg, 1.56 mmol) was added and the reaction mixture was heated under reflux for 2 h. After cooling to room temperature, all ODCB was removed in vacuo. After repetitive column chromatography (silica gel; CS_2/cyclohexane = 1:4) *(CAUTION! The column should be poured in cyclohexane since CS_2 is extremely flammable; silica gel grade I is sufficient to ignite CS_2)* pure **5** was obtained as a brown solid. This was dissolved and precipitated using CS_2/pentane, washed with pentane (2 ×), and dried overnight in a vacuum oven (T = 50 °C) yielding the pure azafulleroid (255 mg, 268 μmol, 18 %). m.p.: 201.7–202.8 °C. ^1H NMR (CS_2, 500 MHz), δ [ppm]: 7.42 (t, J = 8.0, 1H), 7.38–7.37 (m, 2H), 6.97–6.95 (m, 1H), 5.03 (s, 2H), 4.07–4.03 (m, 2H), 1.91 (sep, J = 6.1, 1H), 1.76–1.58 (m, 4H), 1.57–1.49 (m, 4H), 1.16–1.10 (m, 6H). ^{13}C NMR (CS_2, 125 MHz), δ [ppm]: 159.53, 147.58, 146.09, 144.88, 144.51, 144.37, 144.26, 144.11, 143.98, 143.90, 143.64, 143.47, 143.37, 143.23, 143.05,

  1616-301X/01/0510-0379 $ 17.50+.50/0

142.94, 142.75, 142.65, 142.64, 142.52, 141.23, 140.66, 140.63, 139.14, 138.33, 138.09, 138.01, 137.67, 137.35, 137.02, 136.07, 135.47, 133.50, 129.65, 121.04, 115.10, 113.91, 70.08, 54.78, 39.70, 30.96, 29.55, 24.48, 23.76, 14.69, 11.70. FTIR (KBr), ν [cm^{-1}]: 1264 (s, ArOR), 525 (s, [60]fullerene). UV-vis (toluene), ν [cm^{-1}]: 341 (ε = 426 000 $M^{-1}cm^{-1}$), 437 (sh), 551 (ε = 13 900 $M^{-1}cm^{-1}$). MALDI-TOF MS: Calcd. for $^{12}C_{75}H_{23}NO$ (M^-): *m/z* = 953.2. Found: *m/z* = 953.7. Anal. calcd. for $C_{75}H_{23}NO$: C, 94.42 %; H, 2.43 %; N, 1.47 %. Found: C, 94.48 %; H, 2.39 %; N, 1.55 %.

N-3-(2-ethylhexyloxy)benzyl ketolactam (**6**): C_{60} (1.08 g, 1.5 mmol) was dissolved in ODCB (200 mL), degassed (3 ×), and heated under reflux under an atmosphere of nitrogen. 3-(2-Ethylhexyloxy)benzyl azide (408 mg, 1.58 mmol) was added and the reaction was allowed to proceed for 2 h under reflux. After cooling to room temperature, all ODCB was removed in vacuo. Column chromatography (silica gel; CS_2/cyclohexane = 1:4) *(CAUTION! The column should be poured in cyclohexane since CS_2 is extremely flammable; silica gel grade I is sufficient to ignite CS_2)* gave a mixture consisting of C_{60} and [5,6]-3-(2-ethylhexyloxy)-benzyl azafulleroid. This mixture was redissolved in ODCB (200 mL) and irradiated with a 400 W flood lamp using a sheet of Kapton 500HN as UV filter, while a slow stream of oxygen was bubbled through the reaction mixture. HPLC (Cosmosil; toluene/cyclohexane = 1:3) indicated complete reaction in 2 h. Removal of the solvent in vacuo and column chromatography (silica gel; CS_2 to remove the starting fullerene, followed by silica gel; toluene/cyclohexane = 1:1) afforded the pure ketolactam fraction. After removal of the solvent, the product was precipitated from CS_2/pentane, washed with pentane (2 ×) and dried overnight in a vacuum oven (T = 50 °C) yielding the pure product (269 mg, 18 % based on [60]fullerene) as a brown solid. m.p.: 129.7–131.2 °C. ^{1}H NMR (CS_2, 500 MHz), δ [ppm]: 7.31 (t, J = 8.0, 1H), 7.13–7.12 (m, 2H), 6.87 (dd, J = 7.5, J = 2.0, 1H), 6.38 (d, J = 15.0, 1H), 5.38 (d, J = 15.0, 1H), 3.95–3.94 (m, 2H), 1.84 (hep, J = 6.0, 1H), 1.67–1.52 (m, 4H), 1.50–1.44 (m, 4H), 1.10–1.05 (m, 6H). ^{13}C NMR (CS_2, 125 MHz), δ [ppm]: 194.78, 160.71, 159.56, 149.52, 148.95, 147.62, 147.17, 147.13, 147.08, 146.49, 146.31, 146.14, 146.03, 145.89, 145.82, 145.79, 145.73, 145.55, 145.48, 145.14, 145.10, 145.00, 144.94, 144.74, 144.62, 144.27, 144.18, 144.08, 143.98, 143.88, 143.85, 143.73, 143.56, 143.53, 143.40, 143.38, 143.27, 143.18, 142.56, 141.49, 141.03, 140.95, 140.61, 140.44, 140.17, 139.61, 139.25, 139.02, 138.61, 137.94, 137.51, 136.35, 135.77, 135.72, 135.42, 134.85, 133.79, 133.54, 132.92, 132.06, 131.72, 129.89, 128.69, 120.49, 114.67, 114.29, 70.10, 53.99, 39.62, 30.91, 29.51, 24.43, 23.75, 14.69, 11.67. FTIR (KBr), ν [cm^{-1}]: 1727 (s, CO), 1689 (s, CO (amide)), 1260 (m, ArOR), 522 (m, [60]fullerene); UV-vis (toluene), ν [cm^{-1}]: 333 (ε = 488 000 $M^{-1}cm^{-1}$), 433 (ε = 44 400 $M^{-1}cm^{-1}$), 619 (ε = 4 560 $M^{-1}cm^{-1}$), 698 nm (ε = 4 410 $M^{-1}cm^{-1}$). MALDI-TOF MS: Calcd for $^{12}C_{75}H_{23}NO_3$ (M^-): *m/z* = 985.2. Found: *m/z* = 985.8. Anal. calcd. for $C_{75}H_{23}NO_3$: C, 91.36 %; H, 2.35 %; N, 1.42 %. Found: C, 91.42 %; H, 2.35 %; N, 1.41 %.

Received: February 14, 2001
Final version: June 8, 2001

[1] G. Yu, J. Gao, J. C. Hummelen, F. Wudl, A. J. Heeger, *Science* **1995**, *270*, 1789.
[2] N. S. Sariciftci, A. J. Heeger, in *Handbook of Organic Conductive Molecules and Polymers* (Ed: H. S. Nalwa), Vol. 1, John Wiley & Sons, New York **1997**.
[3] a). C. J. Brabec, N. S. Sariciftci, J. C. Hummelen, *Adv. Funct. Mater.* **2001**, *11*, 15. b). C J. Brabec, N. S Sariciftci, in *Conjugated Polymers* (Eds: G. Hadziannou, P. van Hutten), Wiley-VCH, Weinheim **1999**.
[4] S. E. Shaheen, C. J. Brabec, F. Padinger, T. Fromherz, J. C. Hummelen, N. S. Sariciftci, *Appl. Phys. Lett.* **2001**, *78*, 841.
[5] C. J. Brabec, S. E. Shaheen. T. Fromherz, F. Padinger, J. C. Hummelen, A. Dhanabalan, R. A. J. Janssen, N. S. Sariciftci, *Synth. Met.*, in press.
[6] L. H. Campbell, T. W. Hagler, D. L. Smith, J. P Ferraris, *Phys. Rev. Lett.* **1996**, *76*, 1900.
[7] C. M. Heller, I. H. Campbell, D. L. Smith, N. N. Barashkov, J. P. Ferraris, *J. Appl. Phys.* **1997**, *81*, 3217.
[8] I. D. Parker, *J. Appl. Phys.* **1994**, *75*, 1656.
[9] H. Antoniadis, B. R. Hsieh, M. A. Abkowitz, M. Stolka, S. A. Jenekhe, *Polym. Prepr.* **1993**, *34*, 490.
[10] S. Karg, W. Riess, V. Dyakonov, M. Schwoerer, *Synth. Met.* **1993**, *54*, 427.
[11] J. C. Hummelen, B. W. Knight, F. Lepec, F. Wudl, J. Yao, C. L. Wilkins, *J. Org. Chem.* **1995**, *60*, 532.
[12] C. J. Brabec, F. Padinger, N. S. Sariciftci, J. C. Hummelen, *J. Appl. Phys.* **1999**, *85*, 6866.
[13] P. L. Burn, A. Kraft, D. R. Baigent, D. D. C. Bradley, A. R. Brown, R. H. Friend, R. W. Gymer, A. B. Holmes, R. W. Jackson, *J. Am. Chem. Soc.* **1993**, *115*, 10 117.
[14] A. van Oeveren, J. F. G. A. Jansen, B. L. Feringa, *J. Org. Chem.* **1994**, *59*, 5999.
[15] S. G Alvarez, M. T. Alvarez, *Synthesis* **1997**, 413.
[16] J. C. Hummelen, M. Prato, F. Wudl, *J. Am. Chem. Soc.* **1995**, *117*, 7003.
[17] T. Grösser, M. Prato, V. Lucchini, A. Hirsch, F. Wudl, *Angew. Chem. Int. Ed. Engl.* **1995**, *34*, 1343.
[18] This has also been determined for the MEM-ketolactam of reference [16] (J. C. Hummelen, B. Knight, F. Wudl, personal communication **1995**).
[19] a) H. Irngartinger, P. W. Fettel, T. Escher, P. Tinnefeld, S. Nord, M. Sauer, *Eur. J. Org. Chem.* **2000**, 455. b) P. de la Cruz, E. Espíldora, J. J. García, A. de la Hoz, F. Langa, N. Martín, L. Sánchez, *Tetrahedron Lett.* **1999**, *40*, 4889.
[20] T. Da Ros, M. Prato, M. Carano, P. Ceroni, F. Paolucci, S. Roffia, *J. Am. Chem. Soc.* **1998**, *120*, 11 645.
[21] J.-P. Bourgeois, P. Seiler, M. Fibbioli, E. Pretsch, F. Diederich, L. Echegoyen, *Helv. Chim. Acta* **1999**, *82*, 1572.
[22] *Handbook of Chemistry and Physics*, 75th ed. (Ed: D. R. Lide), CRC Press, Boca Raton, FL **1995**, pp. 12–113.
[23] L. J. Brillson, *Surf. Sci. Rep.* **1982**, *2*, 145.
[24] B. W. Hoogenboom, R. Hesper, L. H. Tjeng, G. A. Sawatzky, *Phys. Rev. B* **1998**, *57*, 11 939.
[25] T. R. Ohno, Y. Cehn, S. E. Harvey, G. H. Kroll, J. H. Weaver, R. E. Haufler, R. E. Smalley, *Phys. Rev. B* **1991**, *44*, 13 747.
[26] R. Hespers, *Ph.D. Thesis*, Rijksuniversiteit Groningen, Groningen, The Netherlands **2000**.
[27] L. H. Tjeng, R. Hesper, A. C. L. Heessels, A. Heeres, H. T. Jonkman, G. A. Sawatzky, *Solid State Commun.* **1997**, *103*, 31.
[28] S. J. Chase, W. S. Basca, M. G. Mitch, L. J. Pilione, J. S. Lannin, *Phys. Rev. B* **1992**, *46*, 7873.
[29] M. R. C. Hunt, S. Modesti, P. Rudolf, R. E. Palmer, *Phys. Rev. B* **1995**, *51*, 10 039.
[30] I. G. Hill, D. Milliron, J. Schwartz, A. Kahn *Appl. Surf. Sci.* **2000**, *166*, 354.
[31] P. W. M. Blom, M. J. M. de Jong, M. G. van Munster, *Phys. Rev. B* **1997**, *55*, 656.
[32] P. W. M. Blom, M. J. M. de Jong, J. J. M. Vleggaar, *Appl. Phys. Lett.* **1996**, *68*, 3308.
[33] H. Neugebauer, C. J. Brabec, J. C. Hummelen, N. S. Sariciftci, *Sol. Energy Mater. Sol. Cells* **2000**, *61*, 35.
[34] D. C. Brune, *Rapid Commun. Mass Spectrom.* **1999**, *13*, 384.

  1616-301X/01/0510-0380 $ 17.50+.50/0